

# GEOMETRY MEETS FEEDBACK LOOPS: SHEARING AND TURBULENCE SELF-REGULATION IN NEGATIVE TRIANGULARITY TOKAMAKS

Rameswar Singh and P H Diamond

Department of Astronomy and Astrophysics, University of California San Diego, USA

Email: rsingh@ucsd.edu

## Abstract

Motivated by the observations of improved confinement in negative triangularity (NT) tokamaks, we studied the effects of triangularity on different elements that play significant roles in the physics of turbulence saturation. In particular, we studied the triangularity effects on ITG linear stability, mean ExB shear, zonal flow shear, and GAM shear. Low  $k_y (< 0.5)$  ITG growth rate is reduced for NT than for PT. This is likely due to reduction in magnetic drift frequency and changes in the toroidal resonances. Mean ExB shear exhibits geometric bifurcation at a critical triangularity  $\delta_{crit} (\leq 0)$ . Thus, the shearing rate is maximal off the outboard mid-plane for NT, while it is maximal on the outboard mid-plane for PT. For up-down asymmetric triangularity, the usual up-down symmetry of the shearing rate is broken. The shearing rate at the outboard mid-plane is lower for NT than for PT suggesting that the shearing efficiency in NT is reduced. Shafranov shift increases the shearing rate at all poloidal angles for all triangularities, due to flux surface compression. Implications of interplay of Shafranov shift and mean  $E \times B$  shear for turbulence stabilization and confinement improvement in high- $\beta_p$  NT and ITB discharges are discussed. Zonal flow residual is lower for NT than for PT. This is due to enhanced neoclassical screening owing to increased trapped fraction. GAM frequency and damping rate is strongly reduced for NT. Feedback loops examined with these ingredients suggest that ITG turbulence in NT is dominantly saturated by GAMs.

## 1. INTRODUCTION

Negative triangularity (NT) discharges have demonstrated H-mode-like pressure and energy confinement times for L-mode-like edge conditions[1, 2, 3, 4, 5]. Improved confinement with an L-mode edge is advantageous to a fusion reactor[6, 7]. This is because NT L-mode is an attractive operation regime that is naturally free of ELMs. Also, NT discharges manifest very weak degradation of confinement with power[1], along with broader scrape off layer (SOL) heat flux widths as compared to conventional PT H-mode cases, reduced fluctuation levels[1, 2, 3, 4], and reduced plasma wall interaction[8]. However, understanding of the physics of confinement improvement and L-H transition in NT is still in its infancy. Improved confinement in L-mode should facilitate easy access to H-mode i.e., with lesser power than the conventional L-H transition threshold. While this is observed at weak negative triangularities ( $\delta_u < -0.18$ ) at any input power. This has been linked to loss of access to 2nd stability region of the infinite- $n$  ideal ballooning modes[9, 10]. This model is built upon a previous study predicting reduced pedestal height, clamped by degraded PB and KBM stability, due to closed access to the 2nd stability region for ballooning modes for NT[11]. Past experience with conventional H-mode discharges suggests that *2nd stability access may not be a necessary requirement for H mode*. Loss of 2nd stability, triggered by changing the squareness of plasma shape, only changes low frequency high amplitude ELMs to high frequency low amplitude ELMs, without eliminating the H-mode[12, 13]. A recent experimental study using ECE-imaging suggests that NT edge pressure is limited by low- $n$  interchange type MHD modes or resistive ballooning modes[14]. Gyrokinetic simulations[4, 15, 16, 17] attribute linear stabilization of trapped electron mode (TEM) or ion temperature gradient (ITG) mode to the observed reduction of turbulence and transport in the core of NT configuration, ignoring the role of secondary modes (zonal flows and GAMs) and mean ExB shear. Clearly, the ideas in the NT landscape are still evolving, and a consensus on confinement and L-H physics is still lacking. This *begs* for a study of the mechanisms of turbulence saturation and transport in NT shapes.

Turbulence saturation results from the feedback of the secondary modes and the mean ExB shear on the turbulence. Here, we focus on *the interplay of NT configuration with secondary mode feedback and shearing*. Mean ExB shear, zonal flow shear[18, 19] and GAM (geodesic acoustic mode) shear are candidate players in the saturation of drift wave turbulence in tokamaks, and also play significant roles in the L-H transition. We report on studies of how each of these changes with varying triangularity, encompassing both positive and negative values. ExB shear associated with these candidates break up turbulent eddies, thus reducing the turbulence coherence length[20]. As a result, transport is reduced, and regulated by zonal flow, mean ExB shear and GAM shear. However, note that the GAM shear is generally expected to be weaker than the zonal flow shear, because GAM has a

finite frequency. Our recent work shows that the *zonal flows are weaker in NT than that in PT due to enhanced neoclassical polarization, from an increase in trapped fraction in NT*[21]. As zonal flow lowers the threshold power for L-H transition[22], the prediction of reduced zonal flows in NT is consistent with the observation of increased power threshold for L-H transition. What happens to GAMs in NT? Here, we show that the *GAM frequency and Landau damping rate is significantly reduced in NT compared to that in PT*. This is due to reduction in both magnetic drift frequency and the parallel sound frequency in NT. As a result GAM shearing is expected to be stronger and more coherent in NT than that in PT.

Note that no validated first principle theory of L-H transition[23] exists. However, the transition is almost always linked to transport bifurcation due to mean ExB shearing[24, 22]. Similarly, core transport barriers in high poloidal beta reversed shear discharges - often called internal transport barriers (ITBs) - are sometimes linked to transport bifurcation induced by the local mean  $E \times B$  shear[25, 26]. Thus,  $E \times B$  shear suppression of turbulence and transport is one of the key element of the physics of transport barriers! Given the significant role of mean  $E \times B$  shear in transport barriers formation one wonders *what happens to the shearing rate when the flux surface shapes changes from the PT to NT*? It is well known that magnetic geometry plays a role in shearing physics[27]. Usually, shearing is considered as a flux surface averaged quantity. Experiments, usually, report the shearing rate at the outboard mid-plane. *Here we study the poloidal structure of the mean  $E \times B$  shearing rate as the flux surface shapes vary from PT to NT*, using Miller's parametrized equilibrium model. This also allows the study of the local parametric dependence of the shearing rate with triangularity gradient, elongation, elongation gradient squareness, squareness gradient and Shafranov shift gradient as the triangularity changes from PT to NT. We show that all these local shaping parameters affect the shearing in a non-trivial way. We found that the mean  $E \times B$  shear at the out board mid-plane is lower for NT than that for PT. The maximal mean shear bifurcates at  $\delta \leq 0$  and the shear is maximal off the mid-plane for NT. The shearing becomes up-down asymmetric for asymmetric flux surfaces owing to different upper and lower triangularities. Triangularity gradient reduces the shearing rate, while elongation and elongation gradient increases the mean shear. Negative squareness eliminates the geometric bifurcation for NT, and narrows the poloidal distribution of the shearing. As a result the flux surface averaged shearing rate becomes lower for negative squareness than that for positive squareness. These results have implications for high poloidal beta ( $\beta_p$ ) ITB discharges. ITB formation in high- $\beta_p$  discharges is frequently linked to transport bifurcation due to turbulence stabilization due to drift reduction/reversal by large Shafranov shift[28, 29]. This interpretation ignores the coupling of mean shear to Shafranov shift effects. Mean  $E \times B$  shear exists in these discharges, like it or not. So, one wonders what happens to mean shear in high Shafranov shift regime? Our analysis shows that *the mean shear increases with increasing Shafranov shift gradient, because of enhanced flux surface compression*. Thus, there is a direct boost of mean shear by the Shafranov shift, which complements the conventionally invoked Shafranov shift effect. This observation and the related physics analysis are other major results of this paper.

The rest of the paper is organized as follows. The magnetic equilibrium is described in Section 2. Effect of triangularity on ITG stability and mixing length estimates is discussed in Section 3. The dependencies of the mean ExB shearing rate on different geometric parameters are calculated in Section 4. Variations of zonal flow shear on triangularity is discussed in Section 5. Effects of triangularity on GAM shear is discussed in Section 6. Finally, the paper concludes with an outlook and suggestions for experiments in Section 7.

## 2. DESCRIPTION OF MAGNETIC EQUILIBRIUM

To specify the flux surface shape, we use the local parametrized model for D shaped plasmas developed by Miller et al[30] and generalized for up-down asymmetric flux surfaces with finite squareness

$$R = R_0(r) + r \begin{cases} \cos(\theta + \sin^{-1} \delta_u(r) \sin \theta) & \forall 0 \leq \theta \leq \pi \\ \cos(\theta + \sin^{-1} \delta_l(r) \sin \theta) & \forall \pi \leq \theta \leq 2\pi \end{cases} \quad (1)$$

$$Z = \kappa(r)r \sin(\theta + \sigma \sin 2\theta). \quad (2)$$

Here  $\delta_u$  is upper triangularity,  $\delta_l$  is lower triangularity,  $\kappa$  is ellipticity or elongation and  $\sigma$  is the squareness of the flux surface. For up-down symmetric flux surfaces, the shape is parametrized by a single triangularity parameter  $\delta = \delta_u = \delta_l$ . Note that  $r$  is the minor radius. This allows for systematic studies of the effects of each parameter upon stability and transport for shaped flux surfaces. Here, we study the effects of each of these shaping parameters on the mean  $E \times B$  shearing rate, zonal flows, GAMs, linear growth rates and the feedback loops. The effects of triangularity receives special focus. The magnetic field is defined in flux coordinates  $(\psi, \theta, \zeta)$  as:  $\vec{B} = I \vec{\nabla} \zeta + \vec{\nabla} \zeta \times \vec{\nabla} \psi$ . The Jacobian  $\mathcal{J}$  of transformation  $\vec{r}(r, \theta, \zeta)$  is defined as  $\mathcal{J} = \frac{\partial \vec{r}}{\partial r} \cdot \frac{\partial \vec{r}}{\partial \theta} \times \frac{\partial \vec{r}}{\partial \zeta} = \frac{1}{\vec{\nabla}_r \cdot \vec{\nabla}_\theta \times \vec{\nabla}_\zeta}$ . For  $\vec{r} = R \sin \zeta \hat{x} + R \cos \zeta \hat{y} + Z \hat{z}$ , with  $R$  and  $Z$  given by equations(1) and (2), the Jacobian  $\mathcal{J}$  of transformation

from toroidal coordinates to orthonormal Euclidean coordinates (spanned by the unit basis vectors  $(\hat{x}, \hat{y}, \hat{z})$ ):

$$\mathcal{J} = R \left( \frac{\partial R}{\partial r} \frac{\partial Z}{\partial \theta} - \frac{\partial R}{\partial \theta} \frac{\partial Z}{\partial r} \right) \quad (3)$$

where

$$\begin{aligned} \frac{\partial R}{\partial r} &= R'_0 + \cos(\theta + \sin^{-1} \delta(r) \sin \theta) - S_\delta \sin(\theta + \sin^{-1} \delta(r) \sin \theta) \sin \theta \\ \frac{\partial R}{\partial \theta} &= -r \sin(\theta + \sin^{-1} \delta(r) \sin \theta) (1 + \sin^{-1} \delta(r) \cos \theta) \\ \frac{\partial Z}{\partial r} &= \kappa (1 + S_\kappa) \sin(\theta + \sigma \sin 2\theta) + \kappa \sigma S_\sigma \sin(2\theta) \cos(\theta + \sigma \sin 2\theta) \\ \frac{\partial Z}{\partial \theta} &= \kappa r \cos(\theta + \sigma \sin 2\theta) (1 + 2\sigma \cos 2\theta) \end{aligned}$$

where  $\delta = \begin{cases} \delta_u & \forall 0 \leq \theta \leq \pi \\ \delta_l & \forall \pi \leq \theta \leq 2\pi \end{cases}$ ,  $R'_0 = \frac{\partial R_0}{\partial r}$  is Shafranov shift gradient,  $S_\kappa = \frac{r}{\kappa} \frac{\partial \kappa}{\partial r}$  is ellipticity gradient,  $S_\delta = \frac{r}{\sqrt{1-\delta^2}} \frac{\partial \delta}{\partial r}$  is triangularity gradient, and  $S_\sigma = \frac{r}{\sigma} \frac{\partial \sigma}{\partial r}$  is squareness gradient. Thus, any thing that depends on the Jacobian  $\mathcal{J}$  depends not only on local triangularity  $\delta$ , ellipticity  $\kappa$  and squareness  $\sigma$  but also on their local radial gradients  $S_\delta$ ,  $S_\kappa$ , and  $S_\sigma$ . Here we assume  $R'_0$ ,  $S_\kappa$  and  $S_\delta$  and  $S_\sigma$  are independent parameters.

### 3. EFFECTS OF TRIANGULARITY ON ITG MODE LINEAR STABILITY AND MIXING LENGTH ESTIMATES

The results of local gyrokinetic simulations of linear ITG mode from the GENE code are shown in figure(1). The figure for the growth rate spectra shows non-monotonous behavior with triangularity  $\delta$ . The linear growth rate for NT is lower than PT for low  $k_y (< 0.5)$  modes. For higher  $k_y (> 0.5)$  this trend reverses and the growth rate for NT becomes higher than that for PT. Similarly, the mixing length spectra exhibits non-monotonous behavior with  $\delta$ . The figure shows that mixing length estimates for low  $k_y (< 0.5)$  is lower for NT than for PT. However for  $k_y > 0.5$  the mixing length estimate for NT is higher than that for PT. Calculations of ballooning mode structure (not shown here) also show that the mode width is higher for NT than for PT for low  $k_y (< 0.5)$  modes and mode width becomes lower for NT than for PT for high  $k_y (> 0.5)$  modes. That is, strongly growing modes are more localized in  $\theta$  than the weakly growing modes. This correlation of growth rate and mode width is as expected from the ballooning mode theory. However, the physics of ITG stability spectra trend with  $\delta$  is not clear as of now. This could be related to reduction of magnetic drift frequency and modifications to the toroidal wave-particle resonances. An analytic theory is desirable.

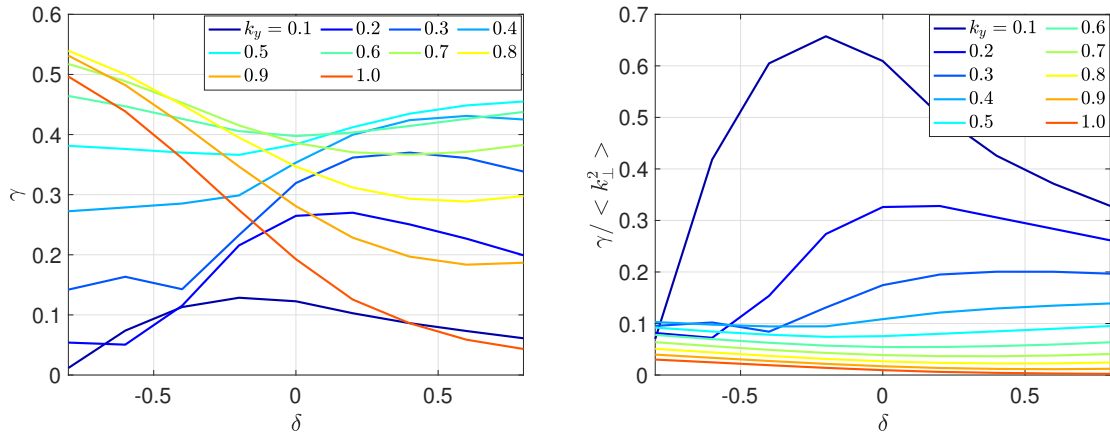


FIG. 1. Linear growth rates of ITG mode and corresponding mixing length estimates obtained from GENE simulations.

## 4. GEOMETRIC DEPENDENCE OF MEAN EXB SHEAR

The Hahm-Burrell formula for the mean  $E \times B$  shearing rate[27] for flute-like modes is obtained from a 2-point correlation calculation for an axisymmetric toroidal system and reads as  $\omega_E = \left(\frac{\Delta\psi_0}{\Delta\zeta}\right) \frac{\partial^2}{\partial\psi^2} \Phi_0(\psi)$ , where  $\Delta\psi_0$  is the turbulence correlation width in poloidal magnetic flux  $\psi$  and  $\Delta\zeta$  is toroidal correlation angle of the ambient fluctuations. The mean electrostatic potential is assumed to be a flux function i.e.,  $\Phi_0 = \Phi_0(\psi)$ . Since, fluctuation diagnostics measure correlation length  $\Delta r$  in the radial co-ordinate  $r$ , we express  $\Delta\psi$  in terms of  $\Delta r$  as  $\Delta\psi = \Delta r \frac{\partial\psi}{\partial r}$ . Similarly, the toroidal correlation angle  $\Delta\zeta$  can be expressed in terms of poloidal correlation angle  $\Delta\theta$  as  $\Delta\zeta = \nu\Delta\theta$ , where  $\nu = \frac{\vec{B} \cdot \vec{\nabla}\zeta}{\vec{B} \cdot \vec{\nabla}\theta} = \frac{I\mathcal{J}}{R^2\psi'}$  is the local safety factor.  $I$  is an effective measure of the total poloidal current outside the flux surface  $\psi = const.$  Notice that,  $\mathcal{J}/\psi'$  is the Jacobian of the flux coordinates  $(\psi, \theta, \zeta)$ . Therefore,  $\frac{\Delta\psi_0}{\Delta\zeta} = \frac{\Delta r}{\Delta\theta} \frac{R^2\psi'^2}{I\mathcal{J}}$ , where  $\psi' = \frac{I(\psi)}{2\pi q(\psi)} \oint d\theta \frac{\mathcal{J}}{R^2}$  is obtained from the definition of the global safety factor  $q$ . Thus, *the magnetic geometry/topology dependence of the mean  $E \times B$  shearing rate enters through the Jacobian  $\mathcal{J}$ , the major radius  $R$  and the radial gradient of poloidal flux i.e.,  $\psi'$  for fixed  $\frac{\partial^2}{\partial\psi^2} \Phi_0(\psi)$* . Clearly,  $\frac{\Delta\psi_0}{\Delta\zeta}$  is not a flux function. So, the mean ExB shear varies with  $\theta$  on a flux surface, such that the shearing rates are *not* symmetric at the inboard and the outboard mid-planes. In-out asymmetry of mean  $E \times B$  shearing rate and fluctuations has been observed in DIII-D PT experiments[31]. The factor  $\frac{R^2\psi'^2}{\mathcal{J}}$  captures the poloidal variation of the mean  $E \times B$  shearing rate on a flux surface. In the following, *we examine how the poloidal structure of the mean shearing rate varies with the flux surface shaping parameters for fixed  $\frac{\partial^2}{\partial\psi^2} \Phi_0(\psi)$ , as set by the radial force balance, and for fixed ratio of radial correlation length to poloidal correlation angle i.e., for fixed  $\frac{\Delta r}{\Delta\theta}$* . The results are inferred from the dependence of the term  $\frac{R^2\psi'^2}{\mathcal{J}}$  on the shaping parameters. The results are summarized in the table(1).

Shaping parameters	Effects on mean $E \times B$ shear			
	$\theta$ - symmetry	flux surface averaged shear $\bar{\omega}_E$	shear at $\theta = 0$ ( $\omega_{E0}$ )	$\delta_{crit}$ for geometric bifurcation
Triangularity $\delta$ (up-down symmetric) [Figure(2)]	$\omega_E(\theta) = \omega_E(-\theta)$ , up-down symmetric, maximum at $\theta \neq 0$ for NT $\implies$ shearing more effective for $k_x \neq 0$ modes	increases with decreasing $\delta$ such that $\bar{\omega}_E(\delta^-) > \bar{\omega}_E(\delta^+)$	decreases with decreasing $\delta$ such that $\omega_{E0}(\delta^-) < \omega_{E0}(\delta^+)$	depends on other shaping parameters ( $\delta_{crit} \leq 0$ )
Triangularity $\delta_u \neq \delta_l$ (up-down asymmetric) [Figure(2)]	$\omega_E(\theta) \neq \omega_E(-\theta)$ , up-down asymmetric, maximum at $\theta > 0$ for NT	increases with decreasing $\delta_{l,u}$ such that $\bar{\omega}_E(\delta_{l,u}^-) > \bar{\omega}_E(\delta_{l,u}^+)$	decreases with decreasing $\delta_{l,u}$ such that $\omega_{E0}(\delta_{l,u}^-) < \omega_{E0}(\delta_{l,u}^+)$	depends on other shaping parameters ( $\delta_{u,crit} \leq 0$ )
Triangularity gradient $S_\delta$		decreases with increasing $ S_\delta $	decreases with increasing $ S_\delta $	decreases (moves towards higher $\delta^-$ )
Shafranov shift gradient $R'_0$ [Figure (3)]		increases with increasing $-R'_0$	increases with increasing $-R'_0$	decreases (moves towards higher $\delta^-$ )
Elongation $\kappa$		increases	increases	no effect
Elongation gradient $S_\kappa$		increases	increases	decreases (moves towards higher $\delta^-$ )
Squareness $\sigma$		increases with increasing $\sigma$ such that $\bar{\omega}_E(\sigma^-) < \bar{\omega}_E(\sigma^+)$	decreases with increasing $\sigma$ such that $\bar{\omega}_E(\sigma^-) > \bar{\omega}_E(\sigma^+)$	increases (moves towards higher $\delta^+$ )
Squareness gradient $S_\sigma$		increases weakly with increasing $S_\sigma$	increases weakly with increasing $S_\sigma$	decreases (moves towards higher $\delta^-$ )

TABLE 1. Summary of effects of shaping parameters on shearing rate.

Notice that the peak shearing bifurcates at a critical triangularity  $\delta_{crit}$ . The shearing peaks symmetrically above and below the outboard mid-plane for up-down symmetric NT flux surface. This up-down symmetry of shearing is broken, and the shearing is strongest above the outboard mid-plane for up-down asymmetric NT shapes. Geometric modifications of the mean shearing can have following important implications.

- Shearing is weaker at the outboard mid-plane for NT than that for PT, at *equal* values of radial force balance  $\frac{\partial^2}{\partial \psi^2} \Phi_0(\psi)$ , while fluctuations balloon at  $\theta = 0$ . The mismatch in ballooning angle and maximum shear location *may reduce the shearing efficiency for NT, even though the flux surface averaged shearing is slightly higher for NT than that for PT*. This may contribute to the increase of the L-H power threshold for NT. This mechanism complements the one based on loss of 2nd stability of ideal MHD ballooning modes.
- The Shafranov shift gradient directly boosts the shearing rate, for all  $\delta$ . This is because of an increase in flux compression with increasing Shafranov shift gradient. Shafranov shift gradient is higher for NT than for PT even for fixed  $\beta_p$ . This means that this effect will be even more important for NT high- $\beta_p$  ITB regimes. Mean shear enhancement by Shafranov shift gradient provides additional turbulence suppression. This mechanism complements the commonly invoked mechanism for confinement improvement in high- $\beta_p$  regimes, which is based on stabilization due to curvature drift reduction/reversal by Shafranov shift. Mean shearing should increase when PT  $\rightarrow$  NT, even at fixed  $\beta_p$ , owing to enhanced Shafranov shift gradient. This in turn can improve confinement and increase  $\beta_p$ . The increase in  $\beta_p$  then drives stronger shearing and Shafranov shift, further increasing confinement and  $\beta_p$ . Thus, *enhanced mean  $E \times B$  shearing by Shafranov shift produces positive feedback in the development of Shafranov shift induced transport bifurcation*[28, 29, 32]. Conversely, the Shafranov shift also has a positive effect on the feedback loop of mean  $E \times B$  shear induced transport bifurcation, not only through a reduction of linear growth rate[33], but also through the enhanced  $E \times B$  shearing rate. See figure(3).

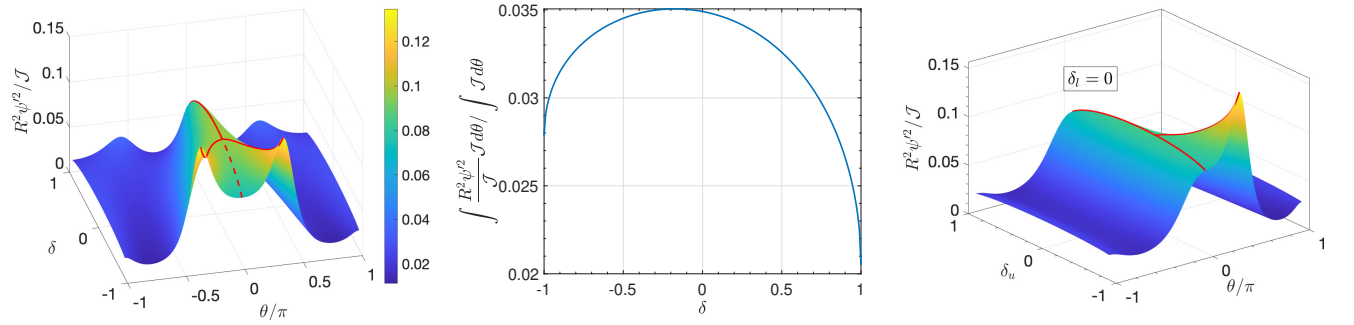


FIG. 2. Left: Structure of mean ExB shearing rate in  $(\theta - \delta)$  space for symmetric flux surfaces. The solid red line tracks the maxima of the shearing rate and the dotted red line tracks the shearing rate at the mid-plane. Middle: Flux surface averaged shearing rate is higher for  $\delta^-$  than that for  $\delta^+$ . Right: Structure of mean ExB shearing rate for asymmetric  $\delta$ . Parameters:  $R'_0 = -0.4$ ,  $S_\delta = 0.8$ ,  $\kappa = 1$ ,  $S_\kappa = 1$ ,  $\sigma = 0$ ,  $S_\sigma = 0$ ,  $\epsilon = 0.18$ ,  $q = 3$ .

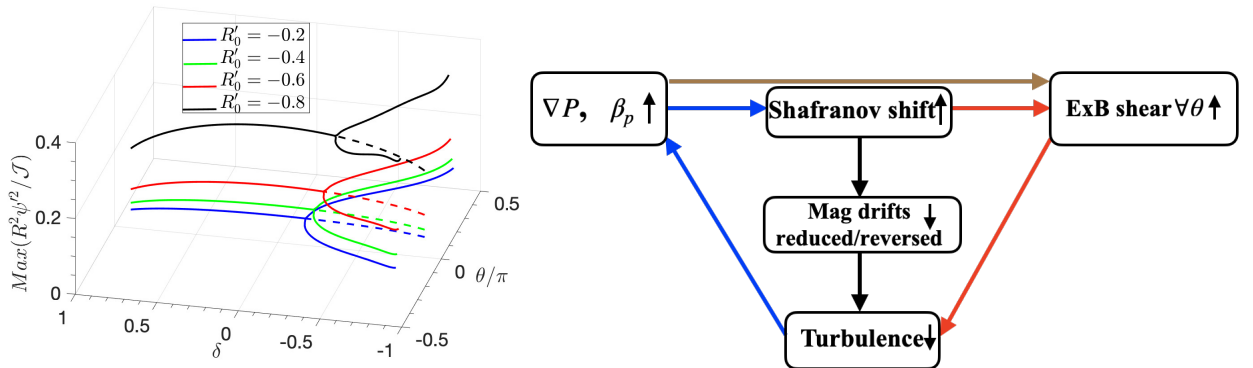


FIG. 3. Left: Shearing rate increases with the Shafranov shift gradient  $R'_0$ . The bifurcation point moves along increasing  $\delta^-$  on increasing  $R'_0$ . Solid lines are the loci of maxima of the mean ExB shearing rate in  $(\theta - \delta)$  space. The dashed lines track the shearing rate at  $\theta = 0$ . Right: Feedback loops of mutual interactions of Shafranov Shift, mean ExB shear and turbulence. Shafranov shift and mean ExB shear reinforces each other to reduce critical  $\nabla P$  for onset of bifurcation to an internal transport barrier (ITB).

## 5. VARIATIONS OF ZONAL FLOW SHEAR WITH TRIANGULARITY

The zonal flow shear is (in part) controlled by the zonal flow screening length, which is primarily determined by the neoclassical dielectric susceptibility[34]. Neoclassical dielectric susceptibility also sets the level of zonal flow residual[35]. So, here we studied flux surface shaping effects on zonal flows residual. To diagnose the physics we studied the shaping effects on susceptibility, zonal flow screening length and particle orbits with a focus on effects manifested by varying triangularity. The results and the physics mechanisms are depicted in figure(4). The main results are:

1. Both classical dielectric susceptibility ( $\chi_{k,cl}$ ) and neoclassical dielectric susceptibility ( $\chi_{k,neo}$ ) *increase* with decreasing triangularity ( $\delta$ ), such that both susceptibilities are higher for negative triangularity than for positive triangularity i.e.,  $\chi_{k,cl}(\delta^-) > \chi_{k,cl}(\delta^+)$  and  $\chi_{k,neo}(\delta^-) > \chi_{k,neo}(\delta^+)$ . Neoclassical susceptibility is always greater than the classical susceptibility i.e.,  $\chi_{k,neo} \gg \chi_{k,cl}$ . As a result, the zonal flow residual is *lower* for negative triangularity than that for positive triangularity. The zonal flow screening length  $l_z$ , given by  $l_z = \sqrt{\chi_{tot}/k_{\perp}^2}$ , is *larger* in negative triangularity than for positive triangularity i.e.,  $l_z(\delta^-) > l_z(\delta^+)$ . Gyrokinetic simulations support the analytic predictions. The zonal flow residual calculated using GENE simulations follows a trend in  $\delta$  similar to that of the analytic predictions.
2. The pitch angle spectra of neoclassical susceptibility  $\chi_{k,neo}$  peaks at the trapped-passing boundary. The dominant contribution to  $\chi_{k,neo}$  is from trapped orbits. The trapped part of the spectrum is *elevated* when  $\delta \rightarrow -\delta$ . The passing part of the spectrum is weakly affected by  $\delta$ .
3. Particle orbit calculations show that *the banana width is reduced in negative triangularity as compared to positive triangularity*. Yet, surprisingly the neoclassical dielectric susceptibility is *higher* in negative triangularity! This is because of the increase in trapped fraction and the bounce angles for negative triangularity, as compared to those for positive triangularity. In fact, *the polarization reduction by banana width reduction is offset by polarization enhancement due to an increase in trapped fraction*.

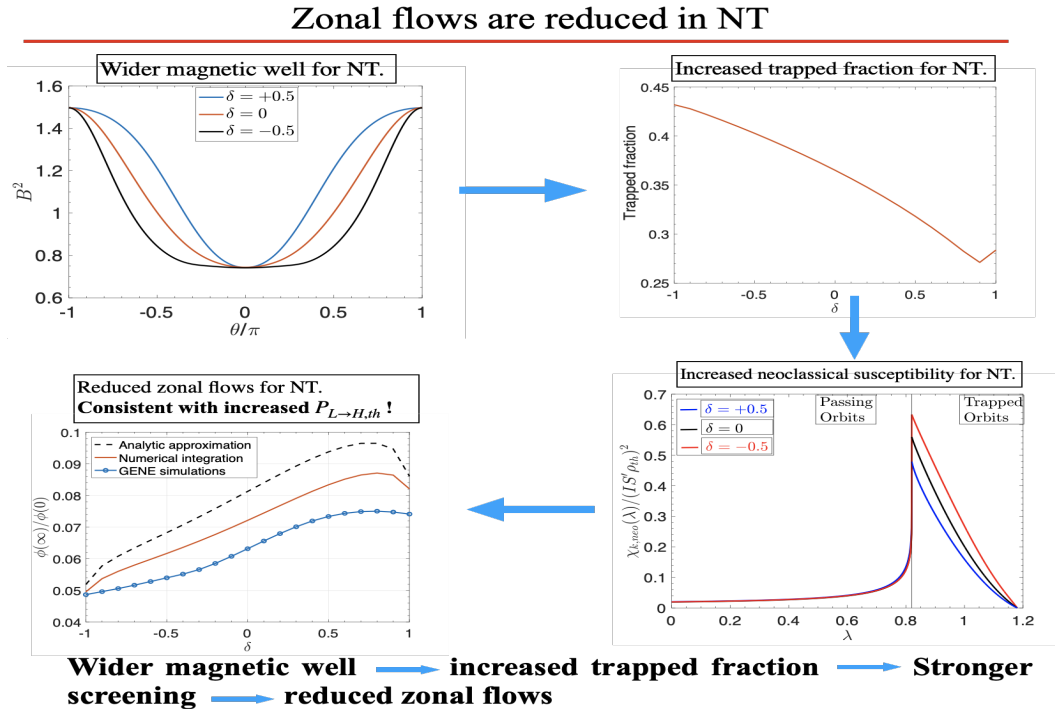


FIG. 4. Residual zonal flow level is lower for NT than for PT[21]. The analytic approximation in the lower left figure corresponds to the small inverse aspect ratio calculations.

## 6. VARIATIONS OF GAM SHEAR WITH TRIANGULARITY

Gyrokinetic GENE simulations show that GAM frequency decreases with decreasing triangularity, such that the frequency is lower for NT compared to that for PT. This implies stronger spatio-temporal coherence of the shearing field in NT, as compared in PT. Analytic calculations reveal that the reduction in frequency for NT is due to reduction in both radial drift frequency and the parallel transit frequency. The GAM Landau damping rate is

shown to be lower for NT as compared to that for PT. Notice that the damping rate is reduced much more strongly ( $\sim 7$  times) than the real frequency, as  $PT \rightarrow NT$ . See figure(5). This implies stronger shearing field for fixed drive in NT. Simultaneous reduction of zonal flow residual and GAM frequency implies that the turbulence is likely saturated by GAMs in NT.

## 7. SUMMARY AND OUTLOOK

Recent positive results from NT discharges have re-ignited the interest in the studies on how flux surface geometry enters the turbulence saturation dynamics. Two big issues staring at the face are: a) the physics explanation of the improved confinement and b) diverging  $P_{th,L \rightarrow H}$  below a critical upper triangularity. Improved confinement has been linked to the linear stabilization of the TEM/ITG mode[4, 15, 3, 16, 36, 37, 17], ignoring the possible role feedback effects of secondary modes. The diverging  $P_{th,L \rightarrow H}$  has been linked to loss of access to infinite- $n$  2nd stability of ideal MHD ballooning modes[9, 10]. But infinite- $n$  modes correspond to very small radial scales. It is unclear why the pedestal cannot survive with these fine scale perturbations. So, here we examined the geometric effects on the ITG turbulence saturation. In particular, we studied the triangularity effects on the major elements of the ITG turbulence saturation dynamics viz., linear stability, mean ExB shear, zonal flow shear, and GAM shear.

In summary, the GAM is likely the dominant player for turbulence regulation in NT as both GAM frequency and damping rates are significantly reduced. Zonal flows are weaker in NT. The improved confinement in NT seems due to the fact that both GAM and zonal flows can drain energy from the turbulence. In PT, the GAM is heavily damped at realistic  $q$ , so only zonal flows can drain energy from the turbulence. This mechanism is distinct from, and complementary to, those based on linear growth reduction. Shafranov shift gradient boosts the mean ExB shear by compressing the flux surfaces. Shafranov shift and mean ExB shear reinforces each other to reduce critical  $\nabla P$  for onset of bifurcation to an internal transport barrier (ITB). The usual up-down symmetry of mean ExB shear is broken for up-down asymmetric triangularities. A higher  $P_{th,L \rightarrow H}$  for NT is suggested, due to 1) reduction of mean ExB shearing at the outboard mid-plane where the turbulent fluctuations balloon and 2) due to reduced zonal flow shear. This picture differs from, and is complementary to that based on infinite- $n$  ideal MHD ballooning mode 2nd stability.

Ongoing efforts include development of analytic theory of ITG stability, nonlinear decorrelation rate, Reynolds power, heat flux, zonal flow damping rate, and GAM damping rate for general magnetic geometry. These will be used to construct a multiple shearing (ZF and GAM) predator-prey model to study the nonlinear saturated states' behavior with the shaping parameters. NT is an interesting test bed for the "conventional wisdom" of turbulence and transport. Any good story should explain both PT and NT observations.

Finally, we present some suggestions for the experimentalists.

- Since the mean shearing is maximal off the outboard mid-plane in NT, the eddy tilting should be maximum off the outboard mid-plane. For up-down symmetric shapes, eddy tilting should maximize symmetrically above and below the outboard mid-plane. For up-down asymmetric flux surface shapes, eddy tilting should maximize above the outboard mid-plane for all positive lower triangularity ( $\delta_l^+$ ), weak negative lower triangularity ( $\delta_l^-$ ) and for all upper triangularities ( $\delta_u$ ). Eddy tilting should maximize below the outward mid-plane for strong  $\delta_l^-$  and all  $\delta_u$ . This can be directly visualized in experiments by gas puff imaging[38]. The poloidal distribution of the tilt angle of the joint pdf of the radial and poloidal velocity fluctuations should also exhibit symmetry/asymmetry about the outboard mid-plane, depending on the flux surface symmetry. This implies that the poloidal envelope of the Reynolds stress should also exhibit similar symmetry/asymmetry due to flux surface shaping effects.
- Re-assess the role of mean  $E \times B$  shear in high- $\beta_p$  reversed shear ITB discharges given that Shafranov shift boosts the mean  $E \times B$  shear.
- Study variation of zonal flow energy to GAM energy when  $PT \rightarrow NT$ , using fluctuation diagnostics.
- Study radial correlation length of zonal flows vs triangularity, and frequency resolved Reynolds stress/Reynolds power vs triangularity, using BES diagnostics.

## ACKNOWLEDGEMENTS

This research was supported by U.S. DOE under Award No. DE-FG02-04ER54738.

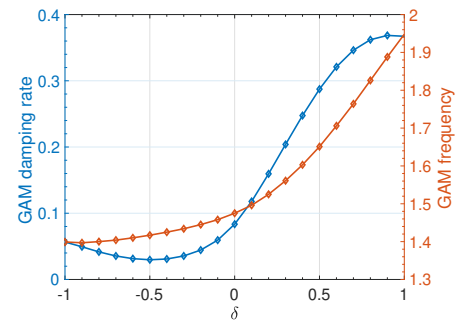


FIG. 5. GAM frequency and Landau damping rates vs triangularity.

## REFERENCES

- [1] M. E. Austin et al. *Phys. Rev. Lett.*, 122:115001, Mar 2019.
- [2] A Marinoni et al. *Physics of Plasmas*, 26(4):042515, 2019.
- [3] M. Fontana et al. *Nuclear Fusion*, 58(2):024002, dec 2017.
- [4] Y Camenen et al. *Nuclear Fusion*, 47(7):510–516, jun 2007.
- [5] S Coda et al. *Plasma Physics and Controlled Fusion*, 64(1):014004, dec 2021.
- [6] M. Kikuchi et al. *Nuclear Fusion*, 59(5):056017, apr 2019.
- [7] C Paz-Soldan. *Plasma Physics and Controlled Fusion*, 63(8):083001, jun 2021.
- [8] W. Han et al. *Nuclear Fusion*, 61(3):034003, feb 2021.
- [9] S Saarelma et al. *Plasma Physics and Controlled Fusion*, 63(10):105006, sep 2021.
- [10] A.O. Nelson et al. *Nuclear Fusion*, 62(9):096020, aug 2022.
- [11] A Merle et al. *Plasma Physics and Controlled Fusion*, 59(10):104001, aug 2017.
- [12] L.L. Lao et al. *Nuclear Fusion*, 39(11Y):1785, nov 1999.
- [13] J.R. Ferron et al. *Nuclear Fusion*, 40(7):1411, jul 2000.
- [14] G You et al. *Physics of Plasmas*, 30(6), 06 2023. 062505.
- [15] A Marinoni et al. *Plasma Physics and Controlled Fusion*, 51(5):055016, mar 2009.
- [16] G Merlo et al. *Plasma Physics and Controlled Fusion*, 63(4):044001, mar 2021.
- [17] J. M. Duff et al. *Physics of Plasmas*, 29(1):012303, 2022.
- [18] P. H. Diamond, S.-I. Itoh, K. Itoh, and T. S. Hahm. *Plasma. Phys. Cont*, 47(5):R35–R161, 2005.
- [19] Rameswar Singh and P H Diamond. *Plasma Physics and Controlled Fusion*, 63(3):035015, jan 2021.
- [20] H. Biglari, P. H. Diamond, and P. W. Terry. *Physics of Fluids B: Plasma Physics*, 2(1):1–4, 1990.
- [21] Rameswar Singh and P.H. Diamond. *Nuclear Fusion*, 62(12):126073, nov 2022.
- [22] Eun-jin Kim and P. H. Diamond. *Phys. Rev. Lett.*, 90:185006, May 2003.
- [23] F Wagner et al. *Phys. Rev. Lett.*, 49:1408–1412, Nov 1982.
- [24] F. L. Hinton. *Physics of Fluids B: Plasma Physics*, 3(3):696–704, 1991.
- [25] K Ida and T Fujita. *Plasma Physics and Controlled Fusion*, 60(3):033001, jan 2018.
- [26] Kenji Imadera and Yasuaki Kishimoto. *Plasma Physics and Controlled Fusion*, 65(2):024003, dec 2022.
- [27] T. S. Hahm and K. H. Burrell. *Physics of Plasmas*, 2(5):1648–1651, 1995.
- [28] S Ding et al. *Physics of Plasmas*, 24(5):056114, 2017.
- [29] J. McClenaghan et al. *Nuclear Fusion*, 59(12):124002, sep 2019.
- [30] R L Miller et al. *Physics of Plasmas*, 5(4):973–978, 1998.
- [31] C L Rettig et al. *Physics of Plasmas*, 5(5):1727–1735, 1998.
- [32] G Staebler et al. *Physics of Plasmas*, 25(5):056113, 2018.
- [33] M A Beer et al. *Physics of Plasmas*, 4(5):1792–1799, 1997.
- [34] Rameswar Singh and P.H. Diamond. *Nuclear Fusion*, 61(7):076009, jun 2021.
- [35] M. N. Rosenbluth and F. L. Hinton. *Phys. Rev. Lett.*, 80(4):724–727, Jan 1998.
- [36] M Fontana et al. *Nuclear Fusion*, 60(1):016006, oct 2019.
- [37] G Merlo et al. *Physics of Plasmas*, 26(10):102302, 2019.
- [38] I. Shesterikov et al. *Nuclear Fusion*, 52(4):042004, mar 2012.